Ab initio calculation of the lithium-tin voltage profile

I. A. Courtney
Department of Physics, Dalhousie University, Halifax, Nova Scotia, B3H 3J5 Canada

J. S. Tse
Steacie Institute for Molecular Science, National Research Council of Canada, Ottawa, Ontario, K1A 0R6 Canada

Ou Mao
Department of Physics, Dalhousie University, Halifax, Nova Scotia, B3H 3J5 Canada

J. Hafner
Department of Theoretical Physics, Technical University Vienna, Vienna A-1040, Austria

J. R. Dahn*
Departments of Physics and Chemistry, Dalhousie University, Halifax, Nova Scotia, B3H 3J5 Canada
(Received 8 April 1998; revised manuscript received 8 June 1998)

An *ab initio* pseudopotential plane-wave method was used to calculate the total energies for several structures (Sn, Li_2Sn_5, LiSn, Li_7Sn_3, Li_5Sn_2, $Li_{13}Sn_5$, Li_7Sn_2, and Li) of the lithium-tin phase diagram. This information was used to determine a theoretical electrochemical voltage profile, which compares well with experiment for $x<2.5$ in Li_xSn. For $x>2.5$, it was found that the equilibrium structures predicted by the phase diagram were not formed in the room-temperature electrochemical cell, which explains why the calculated results are less good there. Calculations of this type are useful for materials research in lithium-ion batteries. [S0163-1829(98)03048-3]

I. INTRODUCTION

A. Lithium-ion intercalation cell

Lithium-ion batteries[1] are the current rechargeable power source of choice for portable electronics devices such as laptop computers and cellular telephones.[2] They can store more energy per weight than their competitors; nickel-metal hydride, nickel-cadmium, or lead-acid.[3] Further increases to the energy density and thermal stability of lithium-ion batteries may lead to their use in electric vehicles.

An ideal lithium-ion cell would be able to pass a large amount of lithium reversibly between anode and cathode, and at a large potential difference. Materials research in this area strives to maximize these quantities in order to produce a battery with increased energy storage capability. The Periodic Table allows for many possible electrode materials, some of which have been discovered and tested, but many which have not. New materials are generally discovered by following general trends that are shown to produce better electrode materials.[4] The advance in performance, coupled with the reduction in cost, of computers has opened the door to a potentially very useful avenue for the materials scientist. This paper demonstrates how well a standard theoretical calculation matches data produced in an electrochemical experiment. This type of approach could be used to predict materials with enhanced energy storage abilities.

B. Total-energy calculations applied to electrochemistry

Several groups have recently performed first-principles calculations of various electrode materials. Deiss *et al.*[5] calculated the average voltage and energy density for $LiC_6/LiMoO_2$ (anode/cathode) cells and $LiC_6/LiNiO_2$ cells. Aydinol *et al.*[6] calculated the average voltages for $Li/LiMO_2$ and $Li/LiCoX_2$ (M=Ti, V, Mn, Co, Ni, Cu, Zn, Al; X=O, S, Se) cells. An approximation made in these calculations is that the transformation from reactant to product is two phase, and so an average voltage can be defined.[6] For example, for $Li/LiCoO_2$ electrochemical cells, the reaction is assumed to be

$$LiCoO_2 \rightarrow CoO_2 + Li. \tag{1}$$

The average voltage is then

$$V = -\Delta G/\Delta x,$$

where Δx refers to the number of lithium transferred [$\Delta x = 1.0$ for Eq. (1)]. We can make a further approximation given that

$$\Delta G = \Delta E + P\Delta V - T\Delta S, \tag{2}$$

where ΔE, the change in internal energy, will be the order of 0.1–4.0 (eV/Li atom), $P\Delta V$ is of the order of 10^{-5} (eV/Li atom), and $T\Delta S$ is the order of the thermal energy (k_BT) which is also much smaller than ΔE at ambient temperatures. Therefore,

$$V = -\Delta E/\Delta x \tag{3}$$

is a good approximation for the electrochemical voltage of the general reaction

$$Li_xX + \Delta x Li \rightarrow Li_{(x+\Delta x)}X. \tag{4}$$

TABLE I. Crystal structure information.

Name	Space group	Lattice constants	Reference
Sn	$I4/amd$	$a=5.83$ Å, $c=3.18$ Å	10
Li_2Sn_5	$P4/mbm$	$a=10.274$ Å, $c=3.125$ Å	11
LiSn	$P2/m$	$a=51.7$ Å, $b=7.74$ Å, $c=3.18$ Å, $\gamma=104.5°$	12
Li_7Sn_3	$P2_1/m$	$a=9.45$ Å, $b=8.56$ Å, $c=4.72$ Å, $\gamma=105.95°$	13
Li_5Sn_2	$R\bar{3}m$	$a=4.74$ Å, $c=19.83$ Å	14
$Li_{13}Sn_5$	$P\bar{3}m1$	$a=4.70$ Å, $c=17.12$ Å	15
Li_7Sn_2	$Cmmm$	$a=9.80$ Å, $b=13.80$ Å, $c=4.75$ Å	16
Li	$Im3m$	$a=3.51$ Å	10

The energy difference ΔE is

$$\Delta E = E_{\text{total}}(\text{Li}_{(x+\Delta x)}X) - E_{\text{total}}(\text{Li}_x X) - \Delta x[E_{\text{total}}(\text{Li})]. \tag{5}$$

Thus, the cell voltage is

$$V = [E_{\text{total}}(\text{Li}_x X) - E_{\text{total}}(\text{Li}_{(x+\Delta x)}X)]/\Delta x - E_{\text{total}}(\text{Li}). \tag{6}$$

A range of anode materials that are currently receiving much interest are tin-oxide composite glasses. This new generation of anode materials have a better energy storage capability than graphite.[7] It has been suggested that the basic reaction mechanism in all of these types of materials is simply an alloying and dealloying reaction between lithium and tin,[8] and thus not an intercalation mechanism. As a first step toward modeling a very complicated system, such as a disordered glass, we submit a first-principles calculation of the lithium-tin voltage profile itself, and compare it to an experimental one.

There are several phase transitions between quite different crystallographic structures, seven to be exact,[9] which makes a first-principles calculation of the lithium-tin system a large undertaking. The experimentally determined structures of these alloy phases, as well as lithium and tin, are listed (along with original references) in Table I. The most lithium-rich phase, $Li_{22}Sn_5$, was not calculated.

II. RESULTS AND DISCUSSION

A. Experimental voltage profile

An electrode of Sn powder (Aldrich, 99.99%$<10\ \mu$m) was prepared by coating a slurry of Sn powder (85% by weight), ''super *S*'' carbon black (10% by weight), and polyvinylidene fluoride (PVDF) (5% by weight) dissolved in *N*-methyl pyrrolidinone on a copper foil substrate. The thickness of the coated film was about 150 μm. After coating, the electrode was dried for 4 h at 106 °C and pressed between plates at 2.0×10^6 Pa. The electrode was cut into 1.44-cm^2 squares and weighed. Coin-type test cells were constructed using this electrode in 2325 (23-mm diameter and 2.5 mm thick) coin cell hardware. The cells used a polypropylene microporous separator, an electrolyte (1-M $LiPF_6$ dissolved in a 30:70-vol % mixture of ethylene carbonate and diethyl carbonate, Mitsubishi Chemical), and a 125-μm-thick, 1.44-cm^2 lithium foil for the negative electrode. Cells were assembled and crimped closed in an argon-filled glove box. Details of cell assembly can be found in Ref. 17. The cells were tested with constant currents (37.2 mA/g).

The voltage profile obtained for one of the cells is shown in Fig. 1. Here the capacity has been rescaled to x in Li_xSn, where $Li_{4.4}Sn$ represents the alloying limit of the Li-Sn phase diagram.[9] The cell did not achieve the maximum capacity of $Li_{4.4}Sn$ as predicted by the equilibrium phase diagram,[9] but only 3.8 equivalents of lithium. This is typical for a Li-Sn voltage curve. This may indicate that the lithium-rich alloy phases are not easily formed in an electrochemical cell at room temperature. Note the well-defined voltage plateaus, which are indicative of two-phase coexistence regions between neighboring phases in the Li-Sn alloy phase diagram.

B. Computational details

The calculations that were performed were based on six two-phase regions according to Eq. (4). The seven line phases have $x=0.0$, 0.4, 1.0, 2.3333, 2.5, 2.6, and 3.5; thus the widths of the two phase regions Δx are $\Delta x=0.4$, 0.6, 1.3333, 0.1667, 0.1, and 0.9. An average voltage was calculated for each of the two-phase regions in accordance with Eq. (6).

The pseudopotential plane-wave method[18] implemented in the Vienna *ab initio* simulation package (VASP) was used to compute the total energies of the Li-Sn alloy phases. VASP performs an iterative diagonalization of the Kohn-Sham

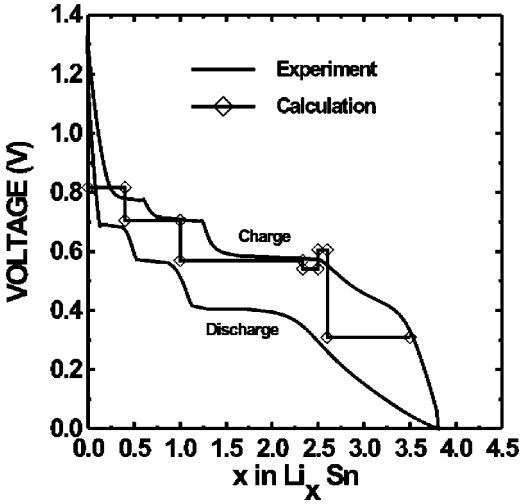

FIG. 1. Experimental and calculated electrochemical voltage profiles for the lithium tin system.

equations of local-density-functional theory based on residuum minimization and optimized charge-density mixing routines.[19] In our calculations, we used the exchange-correlation functional based on the quantum Monte Carlo simulations of Ceperley and Alder as parametrized by Perdew and Zunger.[20] Optimized ultrasoft Vanderbilt pseudopotentials for Li and Sn atoms[21,22] were used in the calculation. The tetrahedron method with Blöch corrections[23] was used in the smearing of the Fermi level. In all of the calculations, the convergence of the total energy with respect to *k*-point sampling and plane-wave energy cutoff have been carefully examined. The final set of energies were computed with an energy cutoff of 200 eV, and the number of *k* points in the irreducible Brillouin zone range from 144 to 310. The calculations have been performed at the experimental volume of the compounds. The reason is that the local-density approximation underestimates the equilibrium atomic volume of the alkali metals (by ~12.5% for Li). This error is partly corrected by including generalized gradient corrections (GGC's) ($V_{\mathrm{Li}}^{\mathrm{GGC}}=19.7$ Å^3, $V_{\mathrm{Li}}^{\mathrm{expt}}=21.4$ Å^3) to the exchange-correlation functional.[24] For Sn, on the other hand, the local-density-approximation (LDA) prediction is more accurate ($V_{\mathrm{SN}}^{\mathrm{LDA}}=33.8$ Å^3, $V_{\mathrm{SN}}^{\mathrm{expt}}=34.2$ Å^3), while the GGC's lead to a overestimate of the equilibrium volume (by +7.2%). Structural predictions, on the other hand are unaffected by the corrections since the GGC's merely add an isotropic term to the pressure.[25] Perhaps with the exception of transition metals,[24] the introduction of GGC's has produced mixed results for main group metals.[24,26] Hence the proper choice of an exchange-correlation functional for Li-Sn alloys leading to correct densities at all compositions remains difficult at the moment. Initial calculations showed that a meaningful voltage profile could not be obtained with the experimental unit-cell sizes and fractional atomic coordinates. The optimization of the atomic positions in the experimental unit cell led to more satisfactory results. The optimized, as well as experimental, atomic positions are shown in Table II. It is observed that the positions of the lithium atoms are affected most in the geometry optimization process, but that the distances from the experimental values are small. This observation is understandable since the intensities of the diffracted x rays in the structural determination are dominated by the much heavier tin atoms. Therefore, the positions for the lighter lithium atoms are often less well defined by the experiment. A tabulation of the calculated total energies for Li, Sn and the Li-Sn alloy phases is shown in Table III. The calculated voltage profile is plotted in Fig. 1.

C. Discussion

The comparison between experiment and calculation is shown in Fig. 1. The results show excellent agreement. The true equilibrium voltage profile would be single valued with respect to charge and discharge, and would lie somewhere in between the charge and discharge curves. Since the experiment was not performed at an infinitesimally slow rate, then we do not measure the true equilibrium voltage profile. The calculation, on the other hand, assumes the equilibrium condition. For $x<0.1$, in the experimental voltage curve of Fig. 1, the voltage does not immediately adopt the plateau of the first two-phase region. This could be due to several reasons; for example, due to a small solubility of lithium in tin, or as a result of small contamination of the tin by oxygen. The later situation would result firstly in the formation of lithia followed by the alloying of lithium with tin.[8] In any event, the modeling of this region could be a worthwhile exercise for future research. For the purpose of this work, however, it was neglected as it only affects a small portion of the voltage profile. The experimental voltage plateaus are well defined up until the formation of Li_7Sn_3. This is consistent with an *in situ* x-ray-diffraction experiment in our earlier work, where the bulk Li-Sn alloy phases Li_2Sn_5 and LiSn were clearly observed.[8] There is a ''voltage spike'' in the calculation at around $x=2.6$, which arises due to the similarity of the stoichiometry of the neighboring phases and the small differences in the total energy between them. The ''jumps'' in voltage which occur at the compositions of the line phases Li_2Sn_5 and LiSn are well matched by the experiment, but the compositions at which the ''jumps'' occur are displaced in the experimental charge curve with respect to the discharge. This is probably caused by the nonzero rate at which the experiment was performed, and further work could address this point. For $2.6<x<3.6$, the calculation predicts another two-phase region and a corresponding plateau, which is not well formed in experiment. We now examine the reasons for this discrepancy.

Figure 2 is an x-ray-diffraction pattern taken of a cell electrode at 0.0 V, equivalent to the compound $Li_{3.8}Sn$. To obtain the electrode for this measurement, a cell was taken into an argon-filled glove box after discharge to 0.0 V. It was then carefully opened and was mounted in a special air-tight x-ray holder with a Kapton window. A Siemens D-5000 diffractometer, equipped with a Cu target x-ray tube and a diffracted beam monochromator, was used to measure the powder pattern of the electrode. According to the Li-Sn phase diagram, this x-ray pattern should show $Li_{22}Sn_5$ and Li_7Sn_2. However, the diffraction pattern does not agree with this prediction, and it shows both sharp peaks and broad oscillations from the sample. The sharp peaks are well indexed to a bcc structure with a lattice constant of $a=3.30$ Å, and the Miller indices are shown next to each peak. We have seen this interesting x-ray pattern in all of our work on Sn containing materials in the structures $Li_xSn(x>2.5)$.[27]

In order to understand the pattern in Fig. 2, we first start by considering the structure of $Li_{22}Sn_5$ as given in the literature.[28] The structure is based on a bcc subcell with a lattice constant $a=3.296$ Å. The tin and lithium atoms are arranged on this bcc network to give a $6\times6\times6$ superstructure with $a=19.78$ Å. The arrangement of Sn atoms is most interesting. All the tin atoms are found on tetrahedra, as shown in Fig. 3(a). The atom at the center of the Sn tetrahedron is a Li atom, and in Fig. 3(b) the tetrahedron itself is shaded, obscuring the Li atom in its center. Figure 3(c) shows a portion of the $Li_{22}Sn_5$ unit cell containing 64 bcc subcells, with Sn tetrahedra indicated. Figure 3(d) shows all the tin atoms in a complete unit cell, and does not show the lithium atoms. All the tin atoms are contained in tetrahedra, which are either isolated, share edges, or share corners.

Given the complex superstructure adopted by the Sn tetrahedra in $Li_{22}Sn_5$, we felt that it was likely that $Li_{4.4}Sn$ prepared at room temperature would not show well-developed long-range order of the Sn tetrahedra. Model cal-

TABLE II. Optimized and experimental atomic coordinates for the alloy phases. The lattice constants were not optimized, so the experimental structure was used for elemental Li and elemental Sn in the calculation (one unique position). Numbers in parentheses are the experimental values if the value was changed during optimization.

Name	Space Group	Atom (site)	x	y	Z
Li_2Sn_5	$P4/mbm$	Sn($8i$)	0.0698 (0.0676)	0.2054 (0.2046)	0.0
		Sn($2d$)	0.0	$\frac{1}{2}$	0.0
		Li($4h$)	0.174 (0.172)	0.674 (0.672)	$\frac{1}{2}$
LiSn	$P2/m$	Sn($1a$)	0.0	0.0	0.0
		Sn($2m$)	0.234 (0.234)	0.0	0.658 (0.666)
		Li($1e$)	$\frac{1}{2}$	$\frac{1}{2}$	0.0
		Li($2n$)	0.271 (0.263)	0.5	0.328 (0.336)
Li_7Sn_3	$P2_1/m$	Sn($2e$)	0.2228 (0.2251)	0.4013 (0.3995)	$\frac{1}{4}$
		Sn($2e$)	0.9153 (0.9179)	0.1955 (0.1974)	$\frac{1}{4}$
		Sn($2e$)	0.4304 (0.4318)	0.1974 (0.1979)	$\frac{1}{4}$
		Li($2e$)	0.724 (0.732)	0.397 (0.392)	$\frac{1}{4}$
		Li($2e$)	0.126 (0.134)	0.007 (0.007)	$\frac{1}{4}$
		Li($2e$)	0.620 (0.622)	0.995 (0.998)	$\frac{1}{4}$
		Li($2e$)	0.312 (0.318)	0.801 (0.803)	$\frac{1}{4}$
		Li($2e$)	0.830 (0.821)	0.812 (0.810)	$\frac{1}{4}$
		Li($2e$)	0.533 (0.533)	0.600 (0.601)	$\frac{1}{4}$
		Li($2e$)	0.015 (0.021)	0.602 (0.606)	$\frac{1}{4}$
Li_5Sn_2	$R\bar{3}m$	Sn($6c$)	0.0	0.0	0.0727 (0.0727)
		Li($6c$)	0.0	0.0	0.355 (0.352)
		Li($6c$)	0.0	0.0	0.213 (0.210)
		Li($3b$)	0.0	0.0	$\frac{1}{2}$
$Li_{13}Sn_5$	$P\bar{3}m1$	Sn($1a$)	0.0	0.0	0.0
		Sn($2d$)	$\frac{1}{3}$	$\frac{2}{3}$	0.7772 (0.7764)
		Sn($2d$)	$\frac{1}{3}$	$\frac{2}{3}$	0.6090 (0.6091)
		Li($1b$)	0.0	0.0	$\frac{1}{2}$
		Li($2c$)	0.0	0.0	0.672 (0.668)
		Li($2c$)	0.0	0.0	0.837 (0.836)
		Li($2d$)	$\frac{1}{3}$	$\frac{2}{3}$	0.946 (0.943)
		Li($2d$)	$\frac{1}{3}$	$\frac{2}{3}$	0.446 (0.445)
		Li($2d$)	$\frac{1}{3}$	$\frac{2}{3}$	0.281 (0.284)
		Li($2d$)	$\frac{1}{3}$	$\frac{2}{3}$	0.109 (0.117)
Li_7Sn_2	$Cmmm$	Sn($4i$)	0.0	0.3189 (0.3127)	0.0
		Sn($4h$)	0.161 (0.153)	0.0	$\frac{1}{2}$
		Li($2a$)	0.0	0.0	0.0
		Li($2c$)	$\frac{1}{2}$	0.0	$\frac{1}{2}$
		Li($4g$)	0.342 (0.359)	0.0	0.0
		Li($4j$)	0.0	0.172 (0.179)	$\frac{1}{2}$
		Li($8p$)	0.187 (0.187)	0.159 (0.154)	0.0
		Li($8q$)	0.342 (0.349)	0.161 (0.165)	$\frac{1}{2}$

culations were therefore undertaken to explore whether a simple random arrangement of Sn tetrahedra on the underlying bcc lattice could explain the pattern observed in Fig. 2.

The Debye scattering formalism, described in Ref. 29, was used to calculate the powder pattern of the model lattices.[27] Figure 4(a) shows the powder diffraction pattern of a tin tetrahedron with an edge length of 4.67 Å, which is the size and shape of the tetrahedron in Fig. 3(b). The first and second peaks in the calculation are at about 23° and 42°, close to the broad peaks observed in the data. This suggests that tin tetrahedra can be responsible for the broad peaks in the experimental pattern.

Figure 4(b) shows a calculation for a lattice consisting of 1000 bcc subunits arranged on a $10\times10\times10$ grid. Tin atoms were placed on tetrahedra as shown in Fig. 3(b), and these tetrahedra were located randomly throughout the lattice. The remaining sites were filled with lithium, and a lithium:tin ratio of 4:1 was used. This pattern shows the same oscilla-

TABLE III. Calculated total energies for Li-Sn alloy phases.

Name	Number of *k* points	Total energy (eV/formula unit)	Total energy per Li_xSn (eV/formula unit)
Li	220	−2.034	N/A
Sn	196	−4.511	−4.511
Li_2Sn_5	144	−28.254	−5.651
LiSn	250	−7.294	−7.294
Li_7Sn_3	250	−32.296	−10.764
Li_5Sn_2	182	−22.389	−11.194
$Li_{13}Sn_5$	310	−57.292	−11.458
Li_7Sn_2	216	−27.135	−13.568

tory pattern from the tin tetrahedra as does Fig. 4(a) and, in addition, the sharp Bragg peaks from the underlying bcc structure. Figure 4(b) also shows the result of the calculation for the same lattice if the lithium atoms are omitted. This is almost identical, because the scattering power of the lithium atom is so small compared to tin. However, the tin-only result shows that the sharp Bragg peaks arise due to the placement of the atoms making up the tin tetrahedra on the underlying bcc lattice. By comparing Figs. 4(a) and 4(b), the effects of the short-range order of the tin atoms can be investigated by doing calculations of tin clusters alone, assuming that the atoms of the clusters ''fit'' onto the underlying bcc lattice.

The calculations in Figs. 4(a) and 4(b) are suggestive that the correct explanation of the diffraction pattern of $Li_{4.4}Sn$ is at hand. However, the first broad peak in the calculation is much broader than experiment [Fig. 4(d)]. The width of the peak can be narrowed if the tin atoms are arranged into larger clusters. Figure 4(c) shows the powder diffraction pattern that an arrangement of five tin tetrahedra would give. Notice that the shape of the first peak matches experiment more closely. This type of calculation was explored for various Li-Sn ratios (Li_xSn, $3.0<x<4.0$), with similar results.

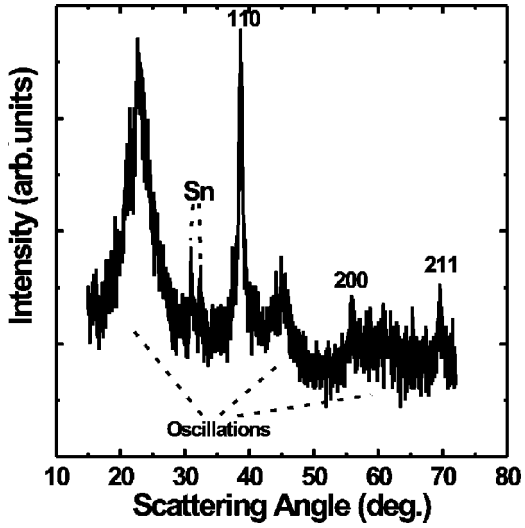

FIG. 2. *Ex situ* diffraction data for an electrode taken from a Li/SnO cell at 0.0 V. The estimated stoichiometry of the alloy is $Li_{3.8}Sn$. Small Sn peaks arise from an incomplete alloying reaction.

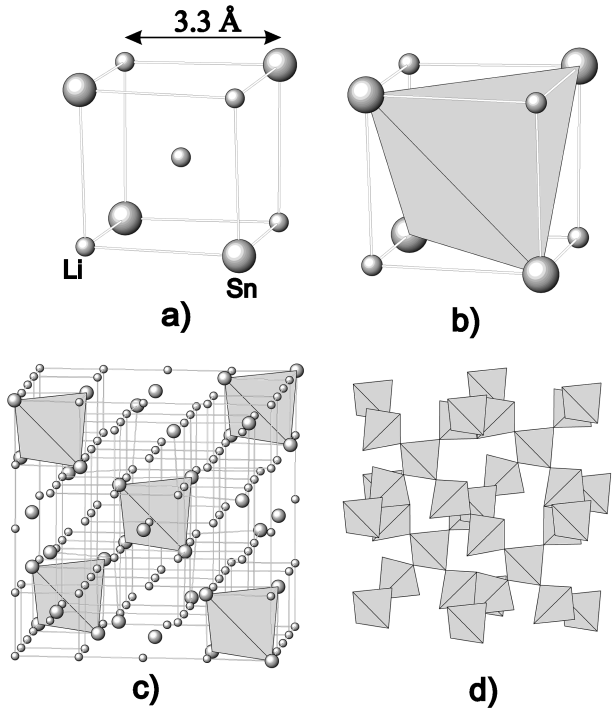

FIG. 3. The structure of $Li_{22}Sn_5$. (a) A bcc unit of the structure which has four tin atoms. (b) Showing how the four tin atoms in (a) are on the corners of a tetrahedron. (c) A portion of the unit cell of $Li_{22}Sn_5$ showing the arrangement of tin tetrahedra and Li atoms. Individual tin atoms are shown where they are in tetrahedra which are not entirely included in the view. Some Li atoms are omitted on the faces of the diagram. (d) All the tin atoms which reside in a unit cell of $Li_{22}Sn_5$ shown in their tetrahedra.

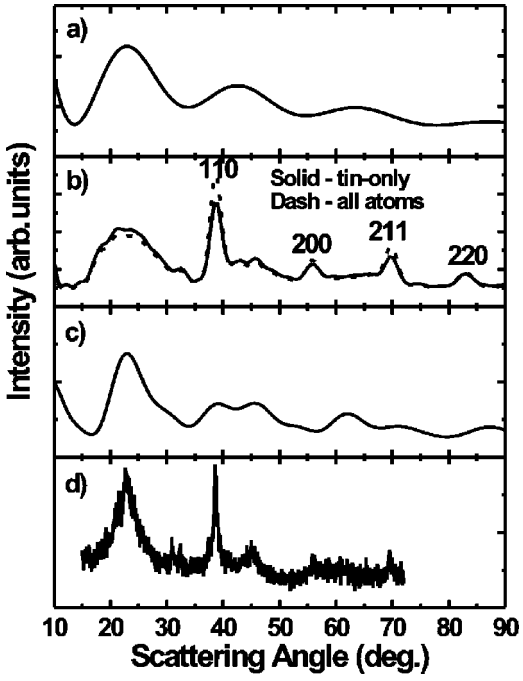

FIG. 4. Powder diffraction patterns calculated for (a) tin tetrahedron, and (b) tin tedrahedra randomly arranged on the underlying bcc lattice (see text). (c) A calculation based on five tin clusters. The experimental data of Fig. 2 are shown for comparison in (d).

The theoretical calculations of the total energies of the Li-Sn alloy phases assumed that they adopted the structures of the bulk equilibrium phases. However, experiment shows that for $x>2.5$, they adopt the structure described above, with Li and Sn atoms on a bcc lattice, having Sn atoms predominantly found in tetrahedra as shown in Fig. 3(a). Therefore, the departure between theoretical and experimental results for the region $x>2.5$ can be appreciated in the context of the structural analysis. This work, therefore, serves as a warning to theorists that equilibrium phases are not always formed in electrochemical cells operating at room temperature.

For $x<2.5$, the calculation and experiment match to an acceptable level for someone interested in the materials research of batteries. It is encouraging that one can perform a calculation to the demonstrated degree of accuracy while dealing with many different and structurally complex lattices. The next step in this type of calculation would be to pursue a first-principles modeling of the tin-oxide composite glass. The tin-oxide composite glasses may be the next generation of anode materials for lithium-ion batteries. The reaction mechanism in these materials is not the traditional intercalation mechanism, which has been well explained. Therefore, the potential for additional insight is vast.

III. CONCLUSION

The electrochemical cell is a very precise, simple, and inexpensive experimental technique by which to measure total energy. Thus the electrochemical cell can test the efficacy of certain *ab initio* calculations with ease. On the other hand, a skilled theorist on a modern computer has at his disposal a potentially very powerful predictive tool for the materials scientist. In this paper we showed the effective use of a first-principles calculation as it is applied to a structurally challenging system, that is, the calculation of the lithium-tin voltage profile.

The calculation and experiment agree well, except in regions where the bulk equilibrium phases do not form in the electrochemical cell. Using x-ray diffraction, we showed that the tin atoms in Li_4Sn prepared at room temperature by electrochemical methods do not adopt the complex superstructure found in $Li_{22}Sn_5$. Instead the tin atoms display only the short-range order characteristic of this phase. Comparisons between experimental voltage profiles, and those calculated based on equilibrium phase diagrams, must recognize the regions where the equilibrium phases are, in fact, formed and the regions where they are not.

ACKNOWLEDGMENTS

The authors acknowledge the Natural Sciences and Engineering Research Council of Canada and 3M Canada Co. for the creation and continued funding of the NSERC/3M Canada Industrial Chair in Materials for Advanced Batteries at Dalhousie University. This work was undertaken under the auspices of the Chair program. The authors also acknowledge both NSERC and 3M Canada Co., as well as the Walter C. Sumner Memorial Trust fund, for support.

*Author to whom correspondence should be addressed.

[1] T. Nagura and K. Tozawa, Prog. Batteries Sol. Cells **9**, 209 (1990); K. Brandt, Solid State Ionics **69**, 173 (1994).
[2] Nomura Research Institute Report, ''Advanced Rechargeable Battery Industry '96'', Nomura Research Institute, Tokyo, Japan 1996 (unpublished).
[3] *Handbook of Batteries*, 2nd ed., edited by D. Linden (McGraw-Hill, New York, 1995).
[4] Jan N. Reimers, J. Power Sources **54**, 16 (1995).
[5] E. Deiss, A. Wokaun, J. L. Barras, C. Daul, and P. Dufek, J. Electrochem. Soc. **144**, 3877 (1997).
[6] M. K. Aydinol, A. F. Kohan, G. Ceder, K. Cho, and J. Joannopoulos, Phys. Rev. B **56**, 1354 (1997).
[7] Y. Idota, A. Matsufuji, Y. Maekawa, and T. Miyasaki, Science **276**, 1395 (1997).
[8] I. A. Courtney and J. R. Dahn, J. Electrochem. Soc. **144**, 2045 (1997).
[9] W. G. Moffat, *The Handbook of Binary Phase Diagrams* (Genium, Schenectady, NY, 1990).
[10] R. W. G. Wyckoff, *Crystal Structures*, 2nd ed. (Krieger, Malabar, FL, 1982), Vol. 1.
[11] D. A. Hansen and L. J. Chang, Acta Crystallogr., Sect. B: Struct. Crystallogr. Cryst. Chem. **25**, 2392 (1978).
[12] W. Muller and H. Schafer, Z. Naturforsch. B **28**, 246 (1973).
[13] W. Muller, Z. Naturforsch. B **29**, 304 (1974).
[14] U. Frank, W. Muller, and H. Schafer, Z. Naturforsch. B **30**, 1 (1975).
[15] U. Frank, W. Muller, and H. Schafer, Z. Naturforsch. B **30**, 6 (1975).
[16] U. Frank and W. Muller, Z. Naturforsch. B **30**, 316 (1975).
[17] A. M. Wilson and J. R. Dahn, J. Electrochem. Soc. **142**, 326 (1995).
[18] G. Kresse and J. Hafner, Phys. Rev. B **48**, 13 115 (1993); **49**, 14 251 (1994).
[19] G. Kresse and J. Furthmuller, Phys. Rev. B **54**, 11 169 (1996).
[20] J. P. Perdew and A. Zunger, Phys. Rev. B **23**, 5048 (1981).
[21] D. Vabderbilt, Phys. Rev. B **41**, 7892 (1990).
[22] G. Kresse and J. Hafner, J. Phys.: Condens. Matter **6**, 8245 (1994).
[23] P. Blöch, O. Jepsen, and O. K. Andersen, Phys. Rev. B **49**, 16 223 (1994).
[24] J. P. Perdew, J. A. Chevary, S. H. Vosko, K. A. Jackson, M. R. Pederson, and D. J. Singh, Phys. Rev. B **46**, 6671 (1992).
[25] K. Seifert, J. Hafner, J. Furthüller, and G. Kresse, J. Phys.: Condens. Matter **7**, 3683 (1995).
[26] A. Garcia, C. Elsässer, J. Zhu, S. G. Louie, and M. L. Cohen, Phys. Rev. B **46**, 9829 (1992).
[27] J. R. Dahn, I. A. Courtney, and Ou Mao, Solid State Ionics (to be published).
[28] E. I. Gladyeshevski, G. I. Oleksiv, and P. I. Kripyakevich, Sov. Phys. Crystallogr. **9**, 269 (1964).
[29] B. E. Warren, *X-Ray Diffraction* (Addison-Wesley, Reading, MA, 1969).